Catalysis Science & Technology

COMMUNICATION

View Article Online
View Journal | View Issue

Cite this: *Catal. Sci. Technol.*, 2016, **6**, 681

Received 28th October 2015,
Accepted 23rd December 2015

DOI: 10.1039/c5cy01845e

www.rsc.org/catalysis

Photocatalytic production of hydrogen peroxide from water and dioxygen using cyano-bridged polynuclear transition metal complexes as water oxidation catalysts†

Yusuke Isaka,[a] Kohei Oyama,[a] Yusuke Yamada,*[b] Tomoyoshi Suenobu[a] and Shunichi Fukuzumi*[acd]

Hydrogen peroxide was produced efficiently from water and dioxygen using $[Ru^{II}(Me_2phen)_3]^{2+}$ (Me_2phen = 4,7-dimethyl-1,10-phenanthroline) as a photocatalyst and cyano-bridged polynuclear transition metal complexes composed of Fe and Co as water oxidation catalysts in the presence of Sc^{3+} in water under visible light irradiation.

Hydrogen peroxide (H_2O_2) has merited increasing attention as an ideal energy carrier alternative to hydrogen, because an aqueous solution of H_2O_2 instead of gaseous hydrogen can be used as a fuel in a one-compartment fuel cell to generate electricity.[1–14] The maximum output potential of an H_2O_2 fuel cell theoretically achievable is 1.09 V which is comparable to that of a hydrogen fuel cell (1.23 V).[1–14] Thus, H_2O_2 production from water (H_2O) and dioxygen (O_2) using solar energy provides an ideally sustainable solar fuel in combination with power generation using an H_2O_2 fuel cell.[15–17] It is highly desired to improve the catalytic activity for the photocatalytic production of H_2O_2 from H_2O and O_2 ($\Delta G°$ = 210 kJ mol^{-1}, eqn (1)) using earth-abundant metal catalysts.[15–17]

$$2H_2O + O_2 \rightarrow 2H_2O_2 \quad \Delta G° = 210 \text{ kJ mol}^{-1} \qquad (1)$$

We report herein the photocatalytic production of H_2O_2 from H_2O and O_2 using $[Ru^{II}(Me_2phen)_3]^{2+}$ (Me_2phen = 4,7-dimethyl-1,10-phenanthroline) as a photocatalyst and structurally-definable and molecularly-ordered metal complexes, *i.e.*, cyano-bridged polynuclear transition metal complexes composed of Fe and Co, as water oxidation catalysts (WOCs) in the presence of Sc^{3+} in water under visible light irradiation. Among various metal complex-based WOCs, metal complexes were found to play in some cases the role of precursors of actual WOCs.[18,19] In contrast, cyano-bridged polynuclear transition metal complexes as they are have been proven to maintain absolutely high catalytic reactivity with high yield and quantum efficiency for water oxidation.[20]

The photocatalytic cycle is shown in Scheme 1, where the excited state of $[Ru^{II}(Me_2phen)_3]^{2+}$ is oxidatively quenched by electron transfer to O_2 to produce $[Ru^{III}(Me_2phen)_3]^{3+}$ and the $O_2^{\bullet-}$–Sc^{3+} complex, which undergoes disproportionation in the presence of H^+ to yield H_2O_2.[15,17] Water is oxidised by $[Ru^{III}(Me_2phen)_3]^{3+}$ in the presence of a heteropolynuclear cyanide metal complex as a WOC to produce O_2.

Heteropolynuclear cyanide complexes take a cubic structure provided that the contained metal ions allow octahedral coordination.[21,22] Both the C and N atoms of cyanide interact with metal ions. When the number of N-bound metal ions is

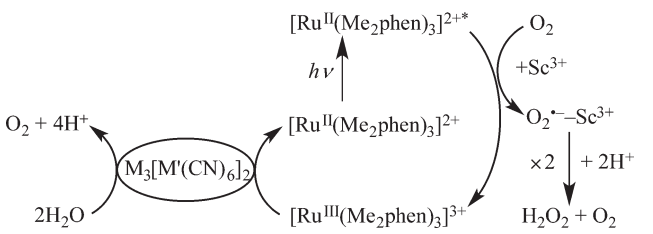

Scheme 1 Catalytic cycle of the photocatalytic production of H_2O_2 from H_2O and O_2 using $[Ru^{II}(Me_2phen)_3]^{2+}$ as a photocatalyst and heteropolynuclear cyanide complexes ($M_3[M'(CN)_6]_2$; M, M′ = different metals) as water oxidation catalysts.

[a] *Department of Materials and Life Science, Graduate School of Engineering, Osaka University, ALCA and SENTAN, Japan Science and Technology Agency (JST), Suita, Osaka 565-0871, Japan. E-mail: fukuzumi@chem.eng.osaka-u.ac.jp*
[b] *Department of Applied Chemistry and Bioengineering, Graduate School of Engineering, Osaka City University, Osaka, 558-0022, Japan*
[c] *Department of Chemistry and Nano Science, Ewha Womans University, Seoul 120-750, Korea*
[d] *Faculty of Science and Technology, Meijo University, ALCA and SENTAN, Japan Science and Technology Agency (JST), Nagoya, Aichi 468-8502, Japan*

† Electronic supplementary information (ESI) available: Experimental section, X-ray diffraction patterns (Fig. S1 and S10b), X-ray fluorescence data (Table S1), DLS data (Fig. S2 and S10c), IR spectra (Fig. S3 and S10a), time courses of H_2O_2 production under various conditions (Fig. S4 and S7–S9), time courses of O_2 evolution (Fig. S5 and S6) and estimation of the amount of evolved O_2. See DOI: 10.1039/c5cy01845e

larger than that of C-bound metal ions, the N-bound metal ions need external ligands such as an aqua ligand to fulfil octahedral coordination.[23,24] The number of external ligands can be controlled by considering charge compensation in a heteropolynuclear complex.[23,24] Thus, heteropolynuclear cyanide complexes composed of different metal ions can be designable heterogeneous catalysts for water oxidation.

A series of heteropolynuclear cyanide metal complexes containing different metal ions, $Co_3[Fe(CN)_6]_2$, $Co_3[Co(CN)_6]_2$, $Cu_3[Co(CN)_6]_2$, $Co[Ni(CN)_4]$, $Fe_3[Cr(CN)_6]_2$, $Mn_3[Fe(CN)_6]_2$, $Co_3[Mn(CN)_6]_2$, $Co_3[Fe(CN)_6]_2$, $Co[Pd(CN)_4]$ and $Co[Pt(CN)_4]$, were prepared according to the literature.[20] Fig. 1 shows the time profiles of the production of H_2O_2 from H_2O and O_2 in an aqueous solution containing $[Ru^{II}(Me_2phen)_3]^{2+}$, $Sc(NO_3)_3$ and a heteropolynuclear cyanide metal complex under visible light irradiation with a xenon lamp using a UV light cut filter ($\lambda > 420$ nm). The amount of produced H_2O_2 was determined by spectroscopic titration with an acidic solution of $[TiO(tpypH_4)]^{4+}$ complex (Ti-TPyP reagent).[25] Among the various heteropolynuclear cyanide complexes, $Fe_3[Co(CN)_6]_2$ exhibited the highest catalytic reactivity.

A series of heteropolynuclear cyanide complexes $(Fe_xCo_{1-x})_3[Co(CN)_6]_2$ (x = 0, 0.10, 0.50, 0.75, 0.90 and 1) were prepared by mixing an aqueous solution of $K_3[Co^{III}(CN)_6]$, $Co^{II}(NO_3)_2$ and $Fe^{II}(ClO_4)_2$ with various Fe/Co ratios of the (Fe_xCo_{1-x}) moiety ranging from 1 : 0 to 0 : 1. All of the synthesised complexes were isostructural with Prussian blue as confirmed by the powder X-ray diffraction patterns (Fig. S1†). A schematic drawing of the complex is shown in Fig. 2. The Co and Fe ion contents of each compound were determined by X-ray fluorescence measurements (Table S1†). The size of $(Fe_xCo_{1-x})_3[Co(CN)_6]_2$ particles remains about the same (260–300 nm) irrespective of the Co-to-Fe ratio as indicated by DLS measurements (Fig. S2†).

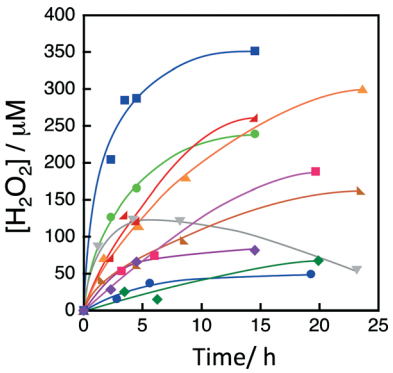

Fig. 1 Time courses of production of H_2O_2 from H_2O and O_2 in an O_2-saturated aqueous solution (2.0 mL) of $[Ru(Me_2phen)_3]^{2+}$ (100 μM), $Sc(NO_3)_3$ (100 mM) and a heteropolynuclear cyanide metal complex (1.0 mg) under photoirradiation of visible light ($\lambda > 420$ nm) with a xenon lamp using a UV light cut filter at room temperature. The employed heteropolynuclear cyanide complexes are $Fe_3[Co(CN)_6]_2$ (blue square), $Co_3[Co(CN)_6]_2$ (red right triangle), $Cu_3[Co(CN)_6]_2$ (green diamond), $Co[Ni(CN)_4]$ (orange regular triangle), $Fe_3[Cr(CN)_6]_2$ (grey inverse triangle), $Mn_3[Fe(CN)_6]_2$ (dark orange right triangle), $Co_3[Mn(CN)_6]_2$ (pink square), $Co_3[Fe(CN)_6]_2$ (light green circle), $Co[Pd(CN)_4]$ (blue circle) and $Co[Pt(CN)_4]$ (purple diamond).

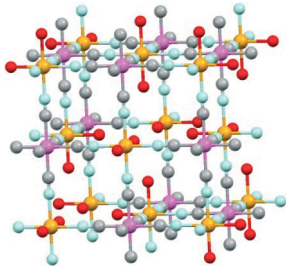

Fig. 2 A schematic drawing of $(Fe_xCo_{1-x})_3[Co(CN)_6]_2$ where x = 0, 0.10, 0.50, 0.75, 0.90 and 1. Ions are colour-coded: N-bound Co^{II} and Fe^{II} (orange), C-bound Co^{III} (pink), C (grey), N (blue) and O (red).

The catalytic reactivity of $(Fe_xCo_{1-x})_3[Co(CN)_6]_2$ with various x values was examined for the production of H_2O_2 from H_2O and O_2 in an O_2-saturated aqueous solution of $[Ru(Me_2phen)_3]^{2+}$ (100 μM), $Sc(NO_3)_3$ (100 mM) and $(Fe_xCo_{1-x})_3[Co(CN)_6]_2$ (1.0 mg) under photoirradiation of visible light with a xenon lamp using a UV-light cut filter ($\lambda > 420$ nm) at room temperature as shown in Fig. S3.† The initial rate of production of H_2O_2 increased with increasing Fe-to-Co ratio in the (Fe_xCo_{1-x}) moiety (Fr_{Fe}), reaching a maximum at Fr_{Fe} = 0.75, and then decreased as shown in Fig. 3. The catalytic reactivity of $(Fe_{0.75}Co_{0.25})_3[Co(CN)_6]_2$ (**1**) was 4.5 and 1.5 times enhanced as compared to those of $Co_3[Co(CN)_6]_2$ and $Fe_3[Co(CN)_6]_2$.

The rate of H_2O_2 production was enhanced 2.9 times when N-bound Co ions in $Co_3[Co(CN)_6]_2$ were thoroughly replaced with Fe ions as shown in Fig. 3. Therefore, the water oxidation reactivity of N-bound Fe ions was higher than that of N-bound Co ions. On the other hand, the peak attributed to CN ligand stretching observed in the IR spectra of $Fe_3[Co(CN)_6]_2$ red-shifted as N-bound Fe^{II} ions were replaced with Co^{II} ions (Fig. S4†). This is because an Fe^{II} ion can accept electrons from bonding orbitals of CN ligands rather easily than a Co^{II} ion because of its low LUMO level. The

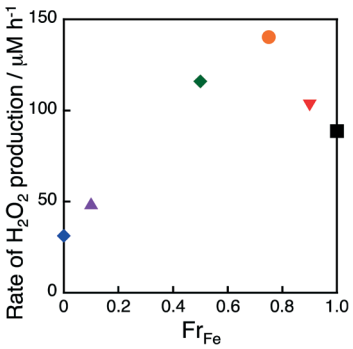

Fig. 3 Initial rates of H_2O_2 production plotted *vs.* fraction of Fe (Fr_{Fe}). H_2O_2 was produced from H_2O and O_2 in an O_2-saturated aqueous solution (2.0 mL) of $[Ru(Me_2phen)_3]^{2+}$ (100 μM), $Sc(NO_3)_3$ (100 mM) and $(Fe_xCo_{1-x})_3[Co(CN)_6]_2$ (1.0 mg), where x = 1 (black square), 0.90 (inverse red triangle), 0.75 (orange circle), 0.50 (green diamond), 0.10 (purple triangle) and 0 (blue diamond) under photoirradiation of visible light ($\lambda > 420$ nm) with a xenon lamp using a UV light cut filter at room temperature. The time courses of H_2O_2 production are shown in Fig. S3.†

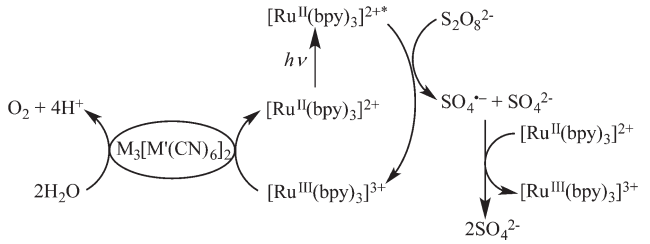

Scheme 2 Photocatalytic cycle of water oxidation with $Na_2S_2O_8$ using $[Ru(bpy)_3]^{2+}$ as a photocatalyst and $(Fe_xCo_{1-x})_3[Co(CN)_6]_2$ as a water oxidation catalyst.

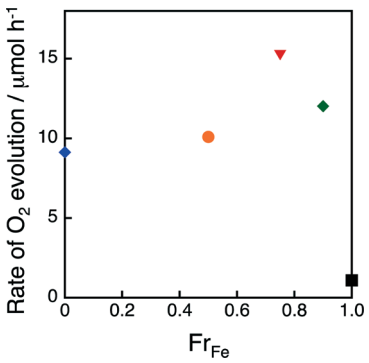

Fig. 4 Initial rates of O_2 evolution plotted *versus* Fr_{Fe}. O_2 evolution was performed by photoirradiation ($\lambda > 420$ nm) of an aqueous phosphate buffer (2.0 mL) containing $Na_2S_2O_8$ (5.0 mM), $Ru[(bpy)_3]^{2+}$ (100 μM) and $(Fe_xCo_{1-x})_3[Co(CN)_6]_2$ (1.0 mg), where x = 1 (black square), 0.90 (green diamond), 0.75 (red inverse triangle), 0.50 (orange circle) and 0 (blue diamond), at pH 8.0 and room temperature. The time courses of O_2 evolution are shown in Fig. S5.†

electron-rich CN ligands can stabilise high-valence metal ions that form in the water oxidation process. Therefore, the volcano-type dependence of the rate of H_2O_2 production on Fr_{Fe} is considered to be a result of those two contradictory effects of Fr_{Fe} on the water oxidation reaction where a complex with a large Fr_{Fe} would contain more active sites for water oxidation while a complex with a small Fr_{Fe} would easily stabilise high-valence metal ions formed during water oxidation.

The catalytic activity of $(Fe_xCo_{1-x})_3[Co(CN)_6]_2$ was also examined in the photocatalytic oxidation of water with persulfate ($Na_2S_2O_8$) using $[Ru(bpy)_3]^{2+}$ (bpy = 2,2′-bipyridine) as a photocatalyst. The photocatalytic cycle is given in Scheme 2, where the excited state of $[Ru(bpy)_3]^{2+}$ was oxidatively quenched by $Na_2S_2O_8$ to produce $[Ru(bpy)_3]^{3+}$, which oxidises water in the presence of $(Fe_xCo_{1-x})_3[Co(CN)_6]_2$ acting as a WOC to evolve O_2. The time courses of O_2 evolution in the photocatalytic water oxidation with $Na_2S_2O_8$ in the presence of $[Ru(bpy)_3]^{2+}$ and $(Fe_xCo_{1-x})_3[Co(CN)_6]_2$ are shown in Fig. S5.† The O_2 evolution rate was maximised at Fr_{Fe} = 0.75 which also gave the most effective WOC for photocatalytic H_2O_2 production (Fig. 4). Catalytic O_2 evolution by water oxidation was also confirmed when $[Ru^{III}(Me_2phen)_3]^{3+}$ was added to an aqueous suspension of **1** at pH 3.0, the same pH condition as that in the H_2O_2 production reaction (Fig. S6†).

The dependence of the rate of production of H_2O_2 on the amount of **1** and $[Ru(Me_2phen)_3]^{2+}$ was examined to obtain the optimised conditions where the amount of **1** is 1.0 mg and $[[Ru(Me_2phen)_3]^{2+}]$ = 100 μM (Fig. S7†). Under such optimised conditions, the quantum efficiency with λ = 450 nm and solar energy conversion efficiency with a solar simulator (HAL-320, Asahi Spectra Co., Ltd.) were determined to be 6.9% and 0.13%, respectively (Fig. S8†).[26]

1 was found to maintain its original catalytic activity for at least 5 repetitive cycles of photocatalytic production of H_2O_2 (Fig. S9†). There was no significant difference between the IR spectra as well as XRD patterns of **1** before the reaction and those of the precipitate obtained after centrifugation of the reaction solution, indicating the robustness of **1** under the reaction conditions (Fig. S10†). DLS data obtained after the reaction (Fig. S10c†) demonstrated no formation of significantly smaller nanoparticles such as metal oxides or hydroxides that could have been *in situ* formed with wide distribution of the particle size in many other cases of Co and other transition metal-based WOCs as reported previously.[27–31] From the results mentioned above, we can conclude that the actual catalytically active species for water oxidation in H_2O_2 production is **1** as it is.[32]

In conclusion, cyano-bridged polynuclear complexes $(Fe_xCo_{1-x})_3[Co(CN)_6]_2$ act as effective water oxidation catalysts for the photocatalytic oxidation of H_2O with O_2 to produce H_2O_2 in an O_2-saturated aqueous solution in the presence of $[Ru(Me_2phen)_3]^{2+}$ and $Sc(NO_3)_3$ under visible light irradiation. The catalytic activity was maximised when the Fe-to-Co ratio in the (Fe_xCo_{1-x}) moiety of $(Fe_xCo_{1-x})_3[Co(CN)_6]_2$ was 0.75. This study provides a unique method to develop efficient catalysts for the photocatalytic water oxidation with O_2 to produce H_2O_2 by changing the ratio of different metals contained in cyano-bridged polynuclear metal complexes.

Acknowledgements

This work was supported by ALCA and SENTAN projects from JST (to S. F. and T. S.) and JSPS KAKENHI (Grant Nos. 24350069 and 15K14223 to Y. Y.).

Notes and references

1 S. Fukuzumi, Y. Yamada and K. D. Karlin, *Electrochim. Acta*, 2012, **82**, 493–511.
2 S. Fukuzumi and Y. Yamada, *Aust. J. Chem.*, 2014, **67**, 354–364.
3 L. An, T. Zhao, X. Yan, X. Zhou and P. Tan, *Sci. Bull.*, 2015, **60**, 55–64.
4 S. Yamazaki, Z. Siroma, H. Senoh, T. Ioroi, N. Fujiwara and K. Yasuda, *J. Power Sources*, 2008, **178**, 20–25.
5 Y. Yamada, Y. Fukunishi, S. Yamazaki and S. Fukuzumi, *Chem. Commun.*, 2010, **46**, 7334–7336.
6 Y. Yamada, S. Yoshida, T. Honda and S. Fukuzumi, *Energy Environ. Sci.*, 2011, **4**, 2822–2825.

7 S. A. M. Shaegh, N. T. Nguyen, S. M. M. Ehteshami and S. H. A. Chan, *Energy Environ. Sci.*, 2012, **5**, 8225–8228.
8 Y. Yamada, M. Yoneda and S. Fukuzumi, *Chem. – Eur. J.*, 2013, **19**, 11733–11741.
9 Y. Yamada, M. Yoneda and S. Fukuzumi, *Inorg. Chem.*, 2014, **53**, 1272–1274.
10 F. Yang, K. Cheng, T. Wu, Y. Zhang, J. Yin, G. Wang and D. Cao, *RSC Adv.*, 2013, **3**, 5483–5490.
11 F. Yang, K. Cheng, X. Xiao, J. Yin, G. Wang and D. Cao, *J. Power Sources*, 2014, **245**, 89–94.
12 X. Xiao, F. Yang, K. Cheng, X. Wang, J. Yin and K. Ye, *J. Electroanal. Chem.*, 2014, **729**, 103–108.
13 Y. Yamada, M. Yoneda and S. Fukuzumi, *Energy Environ. Sci.*, 2015, **8**, 1698–1701.
14 B. Reuillard, S. Gentil, M. Carrière, A. L. Goff and S. Cosnier, *Chem. Sci.*, 2015, **6**, 5139–5143.
15 S. Kato, J. Jung, T. Suenobu and S. Fukuzumi, *Energy Environ. Sci.*, 2013, **6**, 3756–3764.
16 Y. Shiraishi, S. Kanazawa, Y. Kofuji, H. Sakamoto, S. Ichikawa and S. Tanaka, *Angew. Chem., Int. Ed.*, 2014, **53**, 13454–13459.
17 Y. Isaka, S. Kato, D. Hong, T. Suenobu, Y. Yamada and S. Fukuzumi, *J. Mater. Chem. A*, 2015, **3**, 12404–12412.
18 D. Hong, J. Jung, J. Park, Y. Yamada, T. Suenobu, Y. M. Lee, W. Nam and S. Fukuzumi, *Energy Environ. Sci.*, 2012, **5**, 7606–7616.
19 D. Hong, M. Murakami, Y. Yamada and S. Fukuzumi, *Energy Environ. Sci.*, 2012, **5**, 5708–5716.
20 Y. Yamada, K. Oyama, R. Gates and S. Fukuzumi, *Angew. Chem., Int. Ed.*, 2015, **54**, 5613–5617.
21 H. J. Buser, D. Schwarzenbach, W. Petter and A. Ludi, *Inorg. Chem.*, 1977, **16**, 2704–2710.
22 X.-P. Shen, Y.-Z. Li, Y. Song, Z. Xu and G.-C. Guo, *Eur. J. Inorg. Chem.*, 2007, 1698–1702.
23 J. M. Herrera, A. Bachschmidt, F. Villain, A. Bleuzen, V. Marvaud, W. Wernsdorfer and M. Verdaguer, *Philos. Trans. R. Soc., A*, 2008, **366**, 127–138.
24 M. Verdaguer and G. S. Girolami, in *Magnetism: molecules to materials*, ed. J. S. Miller and M. Drillon, Wiley-VCH, Weinheim, 2005, vol. V.
25 C. Matsubara, N. Kawamoto and K. Takamura, *Analyst (Cambridge, U. K.)*, 1992, **117**, 1781–1784.
26 The light intensity was adjusted to 10 mJ cm^{-2} s^{-1} (Air Mass 1.5 (AM1.5)) at the sample position for the whole irradiation area (1.0 × 3.0 cm^2) by using 1 SUN checker (CS-20, Asahi Spectra Co., Ltd.) at room temperature.
27 Q. Yin, J. M. Tan, C. Besson, Y. V. Geletii, D. G. Musaev, A. E. Kuznetsov, Z. Luo, K. I. Hardcastle and C. L. Hill, *Science*, 2010, **328**, 342–345.
28 H. Lv, J. Song, Y. V. Geletii, J. W. Vickers, J. M. Sumliner, D. G. Musaev, P. Kögerler, P. F. Zhuk, J. Bacsa, G. Zhu and C. L. Hill, *J. Am. Chem. Soc.*, 2014, **136**, 9268–9271.
29 J. J. Stracke and R. G. Finke, *ACS Catal.*, 2014, **4**, 79–89.
30 J. J. Stracke and R. G. Finke, *ACS Catal.*, 2014, **4**, 909–933.
31 J. D. Blackmore, R. H. Crabtree and G. W. Brudvig, *Chem. Rev.*, 2015, **115**, 12974–13005.
32 The major reason for the decrease in catalytic activity of the system at prolonged reaction time (Fig. 1) may result from the gradual deactivation of $[Ru^{II}(Me_2phen)_3]^{2+}$; however, no formation of RuO_2 nanoparticles was confirmed by XRD as well as DLS data recorded after the reaction (Fig. S10†).

